文章编号：1001-9014(2024)06-0806-07

DOI:10.11972/j.issn.1001-9014.2024.06.011

Angular-tunable on-chip coding metasurface enabled by phase-change material with immersion liquid

LI Xue-Nan[1,2], ZHAO Zeng-Yue[1*], YU Fei-Long[1], CHEN Jin[1], LI Guan-Hai[1,2,3,4*], LI Zhi-Feng[1], CHEN Xiao-Shuang[1,2,3,4*]

(1. State Key Laboratory of Infrared Physics, Shanghai Institute of Technical Physics, Chinese Academy of Sciences, Shanghai, 200083, China;
2. University of Chinese Academy of Sciences, Beijing, 100049, China;
3. Hangzhou Institute for Advanced Study, University of Chinese Academy of Sciences, Hangzhou, 310024, China;
4. Shanghai Research Center for Quantum Sciences, Shanghai, 201315, China)

Abstract: Metasurfaces provide a potent platform for the dynamic manipulation of electromagnetic waves. Coupled with phase-change materials, they facilitate the creation of versatile metadevices, showcasing various tunable functions based on the transition between amorphous and crystalline states. However, the inherent limitation in tunable states imposes constraints on the multiplexing channels of metadevices. Here, this paper introduces a novel approach - a multi-functional metadevice achieved through the two-level control of the encoding phase-change metaatoms. Utilizing the phase-change material $Ge_2Sb_2Se_4Te_1$ (GSST) and high refractive-index liquid diiodomethane (CH_2I_2), this paper showcases precise control over electromagnetic wave manipulation. The GSST state governs the tunable function, switching it ON and OFF, while the presence of liquid in the hole dictates the deflection angle when the tunable function is active. Importantly, our tunable coding metasurface exhibits robust performance across a broad wavelength spectrum. The incorporation of high refractive-index liquid extends the regulatory dimension of the metadevice, enabling dynamic switching of encoding bit levels. This two-level tunable metadevice, rooted in phase-change materials, presents a promising avenue for the dynamic control of functions.

Key words: coding metasurface, tunable control, phase change material, electromagnetic wave manipulation

基于浸液相变材料的片上角度可调编码超表面

李雪楠[1,2], 赵增月[1*], 郁菲芃[1], 陈 金[1], 李冠海[1,2,3,4*], 李志锋[1], 陈效双[1,2,3,4*]

(1. 中国科学院上海技术物理研究所 红外物理国家重点实验室,中国 上海,200083;
2. 中国科学院大学,中国 北京,100049;
3. 国科大杭州高等研究院,中国 杭州,310024;
4. 上海量子科学研究中心,中国 上海,201315)

摘要:超表面为电磁波的动态调控提供了一个强大平台。超表面与相变材料的结合促进了多功能器件的产生,其基于非晶态和晶态之间转换展示了多种可调的功能。然而,可调状态的内在限制增加了对超器件多路复用的通道约束。介绍了一种通过对编码相变超单元进行二级调控实现多功能超器件的新方法,利用相变材料$Ge_2Sb_2Se_4Te_1$(GSST)和高折射率液体二碘甲烷(CH_2I_2)实现了对电磁波调控的精确控制。设计的超表面

Received date: 2024-02-02, **revised date**: 2024-03-18 **收稿日期**:2024-02-02,**修回日期**:2024-03-18

Foundation items: Supported by the Strategic Priority Research Program (B) of Chinese Academy of Sciences (XDB0580000, XDB43010200); National Natural Science Foundation of China (62222514, 62350073, U2341226, 61991440); National Key Research and Development Program of China (2023YFA1406900); Shanghai Science and Technology Committee (23ZR1482000, 22JC1402900, 22ZR1472700); Natural Science Foundation of Zhejiang Province (LR22F050004); Shanghai Municipal Science and Technology Major Project (2019SHZDZX01); Youth Innovation Promotion Association (Y2021070) and International Partnership Program (112GJHZ2022002FN) of Chinese Academy of Sciences; Shanghai Human Resources and Social Security Bureau (2022670), and China Postdoctoral Science Foundation (2023T160661, 2022TQ0353 and 2022M713261).

Biography: LI Xue-Nan (1996-), female, Shanxi, Ph. D. Research area involves coding metasurface. E-mail: lixuenan@mail.sitp.ac.cn

* **Corresponding authors**: E-mail: zhaozengyue@mail.sitp.ac.cn; ghli0120@mail.sitp.ac.cn; xschen@mail.sitp.ac.cn

由GSST的相态控制可调功能的开启和关闭,当可调功能开启时,微纳孔洞中液体的存在与否决定了偏折的角度。提出的可调编码超表面在宽波谱展现了良好的鲁棒性。与高折射率液体结合拓展了超器件的调控维度,使器件能在不同比特编码间实现动态切换。基于相变材料的二级可调超器件为多功能的动态调控提供了一条可行的路径。

关 键 词:编码超表面;可调控制;相变材料;电磁波调控

中图分类号:O43 **文献标识码**:A

Introduction

Metasurfaces offer distinct advantages, such as compact dimension and low loss, making them widely employed in various applications including metalens, holograms, and optical vortex manipulation [1-4]. Traditionally, metasurface structures are fixed upon array configuration, limiting their adaptability. The growing demand for tunable metasurfaces has emerged with advancements in metasurface technology. The introduction of phase-change materials (PCMs), exemplified by the germanium-antimony-telluride (GST) family and vanadium dioxide (VO_2), has facilitated the development of tunable metadevices [5-6]. PCMs undergo reversible transitions between amorphous and crystalline states, enabling the creation of multifunctional metalens, optical switches, and beam-steering devices [7-9].

Notably, the integration of liquid crystals, diodes, and graphene in coding metasurfaces, where discrete phase shifts manipulate electromagnetic waves, has found extensive applications in tunable devices [10-13]. Moreover, coding metasurfaces utilizing PCMs have been widely adopted for dynamic applications. For example, Huang et al. designed a coding metasurface with switchable beam deflection and focusing based on GST [14], while Lin et al. proposed a coding metasurface based on germanium telluride (GeTe) for dynamic modification of terahertz beams [15]. However, traditional PCM-based metasurfaces are constrained to only two tunable states, pre- and post-phase change. Recent attention has shifted towards miniaturized and highly integrated devices, particularly on-chip devices [16-18]. It offers advantages for the manipulation of in-plane electromagnetic wave propagation. Liquid-based tunable metamaterials, leveraging the ease of liquid addition and removal, have been developed with diverse functionalities. CH_2I_2 with high refractive index has been utilized for aplanatic numerical aperture increasing lenses [19]. Switchable beam-steering has also been achieved through water immersion or drying [20], and the filling height of water in integrated-resonant metaatoms is adjusted to tune the focal length of metalenses [21]. Metasurface with a strong polarization correlation shows different beam reflections in a liquid environment [22]. Water-immersion tuning scheme achieves the switch for both near- and far-field meta-display transformation [23]. Dynamic control of light fields is realized by flowing liquids with different refractive indices over nanostructures [24]. An environment-compliant tunable metaoptics is enabled by a liquid immersion tuning scheme [25]. Despite the versatility demonstrated in different states, the current approaches are limited in their maximal multiplexing channels.

In this work, we present a novel tunable coding metasurface designed for two-level control. Leveraging a combination of GSST and CH_2I_2 liquid, our metasurface regulates in-plane electromagnetic waves across both single and broadband wavelengths. The tunable function is inactive when GSST is in the crystalline state, resulting in an indistinguishable deflection angle for etched holes with or without CH_2I_2. Conversely, when GSST transitions to the amorphous state, the tunable function activates, allowing the conversion of the coding metasurface from 3-bit to 4-bit, accompanied by a change in deflection angle when the etched hole is filled with CH_2I_2. We also discuss the impact of the refractive index of the liquid. This two-level control mechanism introduces a new avenue for designing on-chip dynamic tunable devices.

1 Design and theory

Fig. 1(a) illustrates the schematic of our tunable coding metasurface, designed as a beam deflection device operating at a wavelength of 5.2 μm. The tunable functionality, denoted as ON or OFF, is contingent upon the state of GSST, while the specific deflection angle is determined by the presence or absence of CH_2I_2 liquid within the etched hole. The arrangement of the etched hole along the *y*-direction allows manipulation of the TE polarization (polarized along the *y*-direction) incident wave, propagating along the +*x*-direction. In the amorphous state of GSST, the deflection angle of the electromagnetic wave undergoes alteration upon filling or emptying the CH_2I_2 liquid within the hole. Correspondingly, the phase distribution of the *xy*-plane is depicted in Fig. 1(b). This dynamic modulation of the deflection angle and phase distribution highlights the tunable nature of our coding metasurface, showcasing its ability to control electromagnetic waves based on the state of GSST and the presence of CH_2I_2 liquid.

The metaatom′s schematic diagram, as depicted in Fig. 2(a), comprises the etched hole, GSST, and SiO_2 substrate. GSST is a kind of nonvolatile phase change materials, which phase state can maintain at room temperature. GSST has a large difference in the optical property between the crystalline and amorphous states [26], making it a perfect candidate for the design of tunable metasurfaces. The GSST layer, with a thickness (H) of 2 μm, plays a crucial role in the overall functionality. The dimensions of the etched hole, denoted as length (L) and width (W), are carefully tuned to achieve the desired deflection function. The periodicity of the metaatom, extending along the *y*-direction, is established at

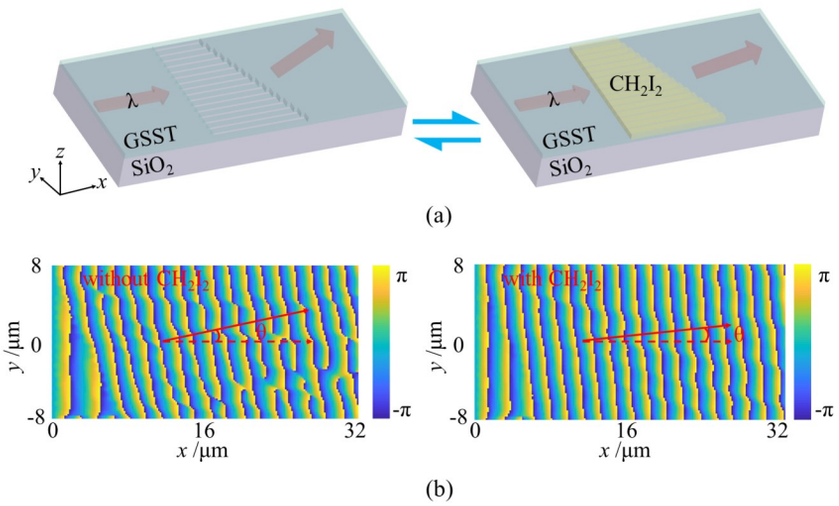

图1 设计的可调编码超表面的示意图:(a)可调编码超表面的结构功能展示(当相变材料GSST处于非晶态时,偏转角度随刻蚀孔中有无CH_2I_2液体而变化);(b)刻蚀孔中有无CH_2I_2液体的*xy*平面的相位分布,其展现了超表面的可调性

Fig. 1 Schematic representation of the designed tunable coding metasurface: (a) illustration of the tunable coding metasurface's structural configuration (When the phase-change material, GSST, is in the amorphous state, the deflection angle varies in response to the presence or absence of CH_2I_2 liquid in the etched hole); (b) phase distribution in the *xy*-plane without or with CH_2I_2 liquid in the etched hole, showcasing the tunability of the metasurface

P = 1 μm. It's necessary to have further consideration on the experimental feasibility. The GSST film can be deposited onto the substrate by thermal co-evaporation, and the desired film can be achieved by controlling the ratio of evaporation rates of two isolated targets of $Ge_2Sb_2Te_5$ and $Ge_2Sb_2Se_5$. The GSST film can be etched via electron beam lithography and reactive ion etching. The GSST film can be changed to the crystalline state by hot-plate annealing at 250°C for 30 min [27]. The addition of CH_2I_2 liquid can by a pipettor and the removal of it can by vaporization [28]. Therefore, the practical experimental is possible for this work. In terms of material properties, the refractive indices of GSST differ in its amorphous and crystalline states, measuring 3.19 and 4.65, respectively, at the operational wavelength of 5.2 μm [26]. Additionally, CH_2I_2 liquid, a key component, exhibits a refractive index of 1.691 at the specified wavelength (5.2 μm) and temperature (20 ℃) [29]. The high refractive index of CH_2I_2 can provide a wide range of phase control, making it a good choice to replace low refractive index water or oil for the design of the tunable metasurface. To determine the refraction angle (θ), we employ the generalized Snell′s law [30], expressed as $\theta = \sin^{-1}(\lambda/(n_t\Gamma))$, where λ represents the designed wavelength, n_t is the effective refractive index of the refraction medium, and Γ signifies the super-period of the designed coding sequence. This formulation guides the modulation of the refraction angle based on the specified parameters, ensuring precise control over the metaatom′s optical properties.

Figs. 2(b) to 2(f) collectively illustrate the four tunable states of the coding metasurface, offering insight into the phase shift and transmittance characteristics of the metaatoms. In the amorphous state of GSST, the phase shift of the metaatom is approximately π/4 and π/8 for the etched hole without or with CH_2I_2 liquid, respectively (Figs. 2(c) and 2(d)). According to the concept of coding metasurface, n-bit coding metasurfaces consist of 2^n coding units with a phase difference of $2\pi/2^n$ [10-12]. Due to the smaller discrete phase difference, higher bit coding provides more precise control of electromagnetic waves and the spurious interference will be effectively suppressed [31-32]. This distinction allows us to define the metaatoms as 3-bit and 4-bit coding configurations, respectively. Conversely, in the crystalline state of GSST, the phase shift remains approximately π/4 for both configurations, regardless of the absence or presence of CH_2I_2 (Figs. 2(e) and 2(f)). Consequently, in this crystalline state, the metaatoms are categorized as 3-bit coding. Notably, during the crystalline state of GSST, the tunable function of the coding metasurface is inactive, signifying that the tunable coding metasurface is in the OFF state.

2 Results and discussions

The validation of our designed tunable coding metasurface was conducted through full-wave simulations. In the amorphous state of GSST, when the tunable function is active, the simulated deflection angles for the etched hole without or with CH_2I_2 liquid are 12.1° and 5.9°, respectively, as depicted in Fig. 3(a). The theoretically calculated deflection angles closely match at 12.4° and 6.2°, respectively. This alignment highlights the dynamic changes in the deflection angle corresponding to the presence or absence of CH_2I_2 in the etched hole. Upon conversion of GSST into the crystalline state, the simulat-

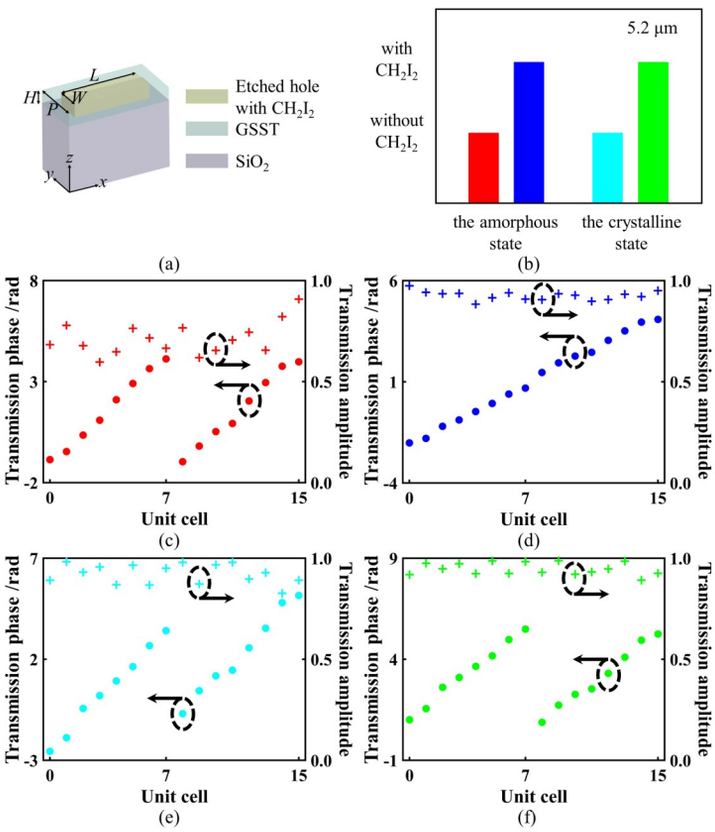

图2 超单元结构及其在不同相变状态下的可调特性:(a)超单元示意图,参数分别为H=2 μm,P=1 μm,W从0变化到1μm,L从0变化到10 μm;(b)可调编码超表面的四个状态;非晶态GSST的编码超单元在刻蚀孔中(c)没有或者(d)有CH_2I_2液体的透射系数和相移;晶态GSST的编码超单元在刻蚀孔中没有(e)或者有(f)CH_2I_2液体的透射系数和相移,以上说明了编码超单元在不同相变状态时的可调特性

Fig. 2 Metaatom configuration and its tunable characteristics across different phase-change states: (a) schematic illustration of the metaatom with parameters H = 2 μm, P = 1 μm, W ranging from 0 to 1 μm, and L from 0 to 10 μm; (b) four states of the tunable coding metasurface; transmittance and phase shift of amorphous state GSST coding metaatoms when the etched hole is without (c) or with (d) CH_2I_2 liquid; transmittance and phase shift of crystalline state GSST coding metaatoms when the etched hole is without (e) or with (f) CH_2I_2 liquid. This highlights the tunable properties of the coding metaatoms in response to different phase-change conditions

ed deflection angles for the etched hole without or with CH_2I_2 liquid are 8.8° and 8.0°, as illustrated in Fig. 3(b). The theoretically calculated deflection angles for both cases are consistent at 8.3°. Remarkably, the presence of CH_2I_2 has minimal impact on the deflection angle in this crystalline state. The phase distribution in the xy-plane for the four different states is presented in Figs. 3(c)~(f). It is evident that the isophase of the wavefront propagating in-plane inclines to varying degrees in each state, resulting in distinct deflection angles in the far field. This observation reinforces the tunable nature of the coding metasurface, demonstrating its ability to dynamically control the direction of electromagnetic waves based on the state of GSST and the presence of CH_2I_2.

The potential influence of evaporation-induced fluctuations in the refractive index of CH_2I_2 liquid on deflection is investigated by simulating four different refractive indices in both amorphous and crystalline states of GSST. The results, presented in Figs. 4(a~d) and 4(e~h), demonstrate the robustness of the coding metasurface in maintaining a consistent deflection effect within a certain range of liquid refractive indices. For the amorphous state of GSST, as the refractive index of the liquid varies between 1.4, 1.6, 1.9, and 2.0, the simulated deflection angles are 6.8°, 6.4°, 5.5°, and 4.7°, respectively (Figs. 4(a~d)). Similarly, in the crystalline state of GSST, the simulated deflection angles for the same range of liquid refractive indices are 8.4°, 8.4°, 7.6°, and 6.4°, as shown in Figs. 4(e~h). Notably, the coding metasurface exhibits a consistent and reliable deflection effect across different liquid refractive indices in both amorphous and crystalline states. Furthermore, the deflection angle decreases with an increase in the liquid refractive index, indicating the sensitivity of the deflection effect to variations in the refractive index of CH_2I_2 liquid within the specified range.

In addition, we delved into the operational bandwidth of the proposed tunable coding metasurface. When

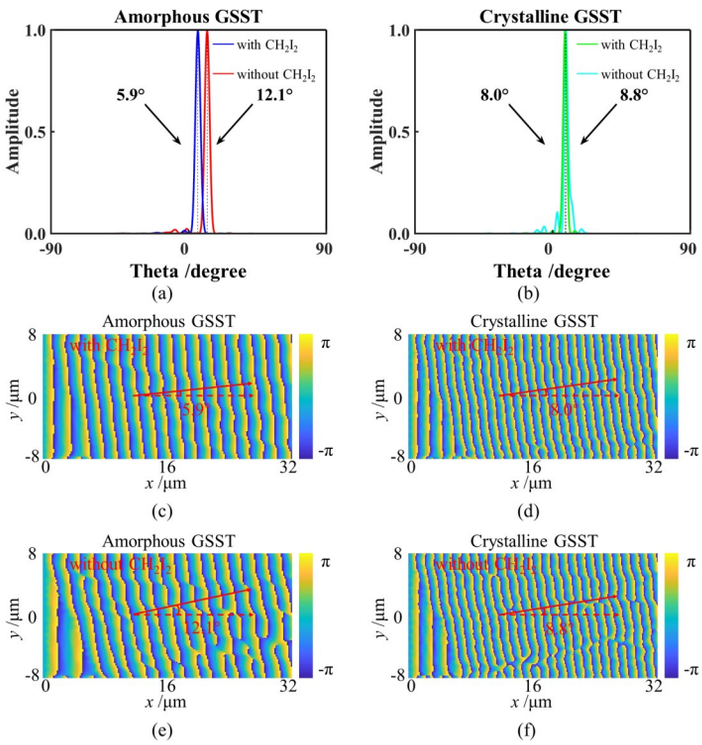

图3 可调编码超表面的偏折功能：(a)当GSST处于非晶态、波长为5.2 μm时，刻蚀孔中有(蓝色线)或者没有(红色线)CH_2I_2液体的模拟远场散射图；作为对照，晶态GSST的散射图展示在(b)中；非晶态GSST刻蚀孔中有(c)或者没有(e)CH_2I_2液体在*xy*平面的相位分布；晶态GSST刻蚀孔中有(d)或者没有(f)CH_2I_2液体在*xy*平面的相位分布。这些结果说明了可调编码超表面在不同条件下的偏转特性

Fig. 3 Deflection function of the tunable coding metasurface: (a) simulated far-field scattering pattern of the etched hole with (blue line) or without (red line) CH_2I_2 liquid at a wavelength of 5.2 μm when GSST is in the amorphous state; For comparison, the scattering pattern of GSST in the crystalline state is also presented in (b); Phase distribution in the *xy*-plane with the etched hole containing (c) or lacking (e) CH_2I_2 liquid in the amorphous state of GSST. Phase distribution in the *xy*-plane with the etched hole containing (d) or lacking (f) CH_2I_2 liquid in the crystalline state of GSST. These results illustrate the deflection characteristics of the tunable coding metasurface under different conditions

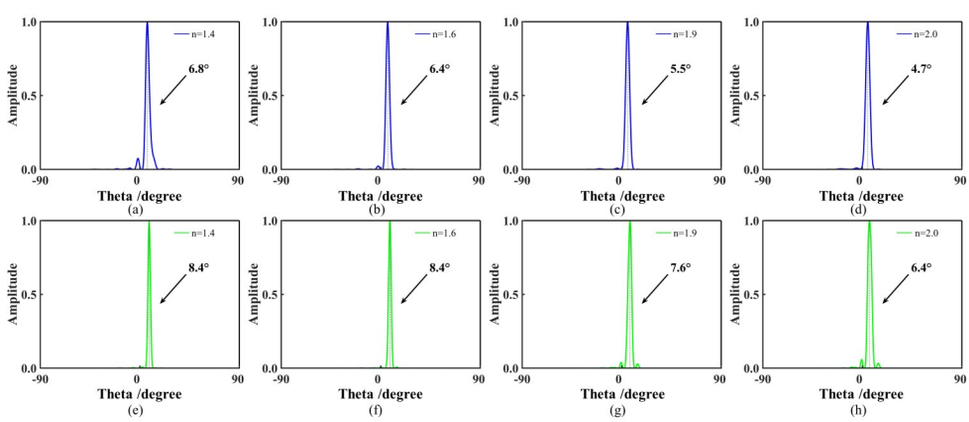

图4 CH_2I_2液体折射率的变化。非晶态GSST(a~d)和晶态GSST(e~h)在液体折射率分别为：1.4，1.6，1.9，2.0时的模拟远场散射图。这些结果证明了CH_2I_2液体折射率的变化对GSST非晶态和晶态散射角度的影响

Fig. 4 Refractive index changes of CH_2I_2 liquid. Simulated far-field scattering patterns of amorphous state GSST (a~d) and crystalline state GSST (e~h) at refractive indices of the liquid: 1.4, 1.6, 1.9, and 2.0, respectively. These results demonstrate the influence of varying refractive indices of CH_2I_2 liquid on the scattering patterns in both amorphous and crystalline states of GSST

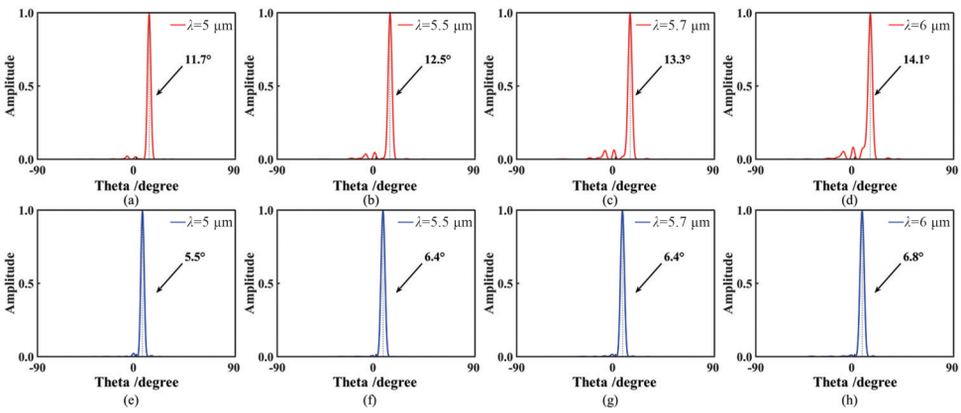

图5　宽带可调编码超表面。非晶态GSST刻蚀孔中没有液体(a~d)或有液体(e~h)的模拟远场散射图。波长分别为5 μm,5. 5 μm,5. 7 μm,6 μm。这些模拟结果显示了编码超表面的宽带可调性,展示了不同波长下的散射角度

Fig. 5　Broadband tunable coding metasurface. Simulated far-field scattering patterns of the etched hole without liquid (a~d) or with liquid (e~h) in the amorphous state of GSST. Wavelengths considered are 5 μm, 5. 5 μm, 5. 7 μm, and 6 μm, respectively. These simulations showcase the broadband tunability of the coding metasurface, highlighting the scattering patterns at different wavelengths

the device operates in the amorphous state of GSST, we found that the working wavelength of the metasurface can be expanded to a broadband range from 5 to 6 μm. The deflection angles of the etched hole without or with liquid at wavelengths of 5 μm, 5. 5 μm, 5. 7 μm, and 6 μm are illustrated in Fig. 5. At these specified wavelengths, the simulated deflection angle varies from 11. 7° to 14. 1° when the etched hole is without liquid, and from 5. 5° to 6. 8° when the etched hole is filled with liquid. According to the generalized Snell′s law, the deflection angle is positive correlation with the working wavelength. Hence, the deflection angle is corresponding increases with the increase of working wavelength. This indicates that the deflection function remains valid across a broadband spectrum. The on-chip photonic device we designed exhibits robust performance, showcasing its suitability for applications requiring reliable and tunable deflection within a broad range of wavelengths.

3　Conclusions

In conclusion, our study successfully achieved two-level control of the coding metasurface, demonstrating versatility in both single and broadband wavelength applications. The tunable function of the on-chip device transitions from OFF to ON when GSST converts from the crystalline to the amorphous state. Under the OFF state, the deflection angle remains consistent whether the etched hole is without or with liquid. Conversely, under the ON state, the deflection angle is switchable based on the presence or absence of liquid in the etched hole. Notably, the deflection effect is robust and can be maintained regardless of changes in refractive index of liquid or operating wavelength, emphasizing the resilience of our on-chip photoelectric devices. Our findings open avenues for dynamic manipulation in on-chip devices, holding potential implications for the advancement of optical computational circuits, on-chip spectrometers, detectors, and other related technologies.

References

[1] Hsiao H H, Chu C H, Tsai D P. Fundamentals and Applications of Metasurfaces [J]. *Small Methods*, 2017, **1**(4): 1600064.
[2] Khorasaninejad M, Capasso F. Metalenses: Versatile multifunctional photonic components [J]. *Science*, 2017, **358**(6367): eaam8100.
[3] Wen D D, Yue F Y, Li G X, *et al*. Helicity multiplexed broadband metasurface holograms [J]. *Nature Communications*, 2015, **6**: 8241.
[4] Ou K, Li G H, Li T X, *et al*. High efficiency focusing vortex generation and detection with polarization-insensitive dielectric metasurfaces [J]. *Nanoscale*, 2018, **10**(40): 19154-19161.
[5] Raoux S, Ielmini D, Wuttig M, *et al*. Phase change materials [J]. *Mrs Bulletin*, 2012, **37**(2): 118-123.
[6] Gong Z L, Yang F Y, Wang L T, *et al*. Phase change materials in photonic devices [J]. *Journal of Applied Physics*, 2021, **129**(3): 030902.
[7] Xu J W, Tian X M, Ding P, *et al*. $Ge_2Sb_2Se_4Te_1$-based multifunctional metalenses for polarization-independent, switchable and dual-mode focusing in the mid-infrared region [J]. *Optics Express*, 2021, **29**(26): 44227-44238.
[8] Michel A-K U, Zalden P, Chigrin D N, *et al*. Reversible optical switching of infrared antenna resonances with ultrathin phase-change layers using femtosecond laser pulses [J]. *ACS Photonics*, 2014, **1**(9): 833-839.
[9] De Galarreta C R, Alexeev A M, Au Y Y, *et al*. Nonvolatile reconfigurable phase-change metadevices for beam steering in the near infrared[J]. *Advanced Functional Materials*, 2018, **28**(10): 1704993.
[10] Cui T J, Qi M Q, Wan X, *et al*. Coding metamaterials, digital metamaterials and programmable metamaterials [J]. *Light: Science & Applications*, 2014, **3**(10): e218.
[11] Liu C X, Yang F, Fu X J, *et al*. Programmable manipulations of terahertz beams by transmissive digital coding metasurfaces based on liquid crystals[J]. *Advanced Optical Materials*, 2021, **9**(22): 2100932.
[12] Huang C, Sun B, Pan W B, *et al*. Dynamical beam manipulation based on 2-bit digitally-controlled coding metasurface [J]. *Scientific Reports*, 2017, **7**: 42302.
[13] Chen H, Lu W B, Liu Z G, *et al*. Microwave programmable graphene metasurface[J]. *ACS Photonics*, 2020, **7**(6): 1425-1435.
[14] Huang X Y, Liu Z X, Lian Y, *et al*. Dynamic beam all-direlectric coding metasurface converter based on phase change materials of GST [J]. *Optics & Laser Technology*, 2023, **159**: 109037.
[15] Lin Q W, Wong H, Huitema L, *et al*. Coding metasurfaces with reconfiguration capabilities based on optical activation of phase-change materials for terahertz beam manipulations[J]. *Advanced Optical Materials*, 2021, **10**(1): 2101699.
[16] Guo Y H, Pu M B, Li X, *et al*. Chip-integrated geometric metasurface as a novel platform for directional coupling and polarization sorting by spin-orbit interaction[J]. *IEEE Journal of Selected Topics in*

Quantum Electronics, 2018, **24**(6): 4700107.
[17] Wang Z, Li T T, Soman A, *et al*. On-chip wavefront shaping with dielectric metasurface [J]. *Nature Communications*, 2019, **10**(1): 3547.
[18] Yang R, Shi Y Y, Dai C J, *et al*. On-chip metalenses based on one-dimensional gradient trench in the broadband visible [J]. *Optics Letters*, 2020, **45**(20): 5640-5643.
[19] Laskar J M, Kumar P S, Herminghaus S, *et al*. High refractive index immersion liquid for superresolution 3D imaging using sapphire-based aplanatic numerical aperture increasing lens optics [J]. *Applied Optics*, 2016, **55**(12): 3165-3169.
[20] Li Z, Wan C W, Dai C J, *et al*. Actively switchable beam-steering via hydrophilic/hydrophobic-selective design of water-immersed metasurface[J]. *Advanced Optical Materials*, 2021, **9**(17): 2100297.
[21] Yao J, Chen M K, Lin R, *et al*. Tunable water-based meta-lens [J]. *Advanced Optical Materials*, 2023, 2300130.
[22] He K, Tang T T, Bi L, *et al*. Polarization-dependent reconfigurable light field manipulation by liquid-immersion metasurface [J]. *Optics Express*, 2023, **31**(9): 13739-13750.
[23] Wan S, Dai C J, Li Z, *et al*. Toward water-immersion programmable meta-display [J]. *Advanced Science*, 2022, **10**(5): 2205581.
[24] Li Q T, van de Groep J, White A K, *et al*. Metasurface optofluidics for dynamic control of light fields [J]. *Nature Nanotechnology*, 2022, **17**(10): 1097-1103.
[25] Li Z, Wan C W, Dai C J, *et al*. Immersion-triggered active switch for spin-decoupled meta-optics multi-display[J]. *Small*, 2022, **18**(50): 2205041.
[26] Zhang Y F, Chou J B, Li J Y, *et al*. Broadband transparent optical phase change materials for high-performance nonvolatile photonics [J]. *Nature Communications*, 2019, **10**(1): 4279.
[27] Shalaginov M Y, An S, Zhang Y, *et al*. Reconfigurable all-dielectric metalens with diffraction-limited performance [J]. *Nature Communications*, 2021, **12**(1): 1225.
[28] Hou B B, Zhang L N. Liquid microdroplet as an optical component to achieve imaging of 100nm nanostructures on a far-field microscope [J]. *Journal of optics*, 2018, **20**(5): 055606.
[29] PRICHARD W H, ORVILLE-THOMAS W J. Infra-red dispersion studies Part 1.-dichloro-, dibromo-, and diiodomethane [J]. *Transactions of the Faraday Society*, 1963, **59**(490): 2218-2227.
[30] Yu N F, Genevet P, Kats M A, *et al*. Light propagation with phase discontinuities: generalized laws of reflection and refraction[J]. *Science*, 2011, **334**(6054): 333-337.
[31] Cheng Q, Zhang L, Dai J Y, *et al*. Reconfigurable intelligent surfaces: simplified-architecture transmitters—from theory to implementations[J]. *Proceedings of the IEEE*, 2022, **110**(9): 1266-1289.
[32] Wang H L, Zhang Y K, Zhang T Y, *et al*. Broadband and programmable amplitude-phase-joint-coding information metasurface [J]. *ACS applied materials & interfaces*, 2022, **14**(25): 29431-29440.